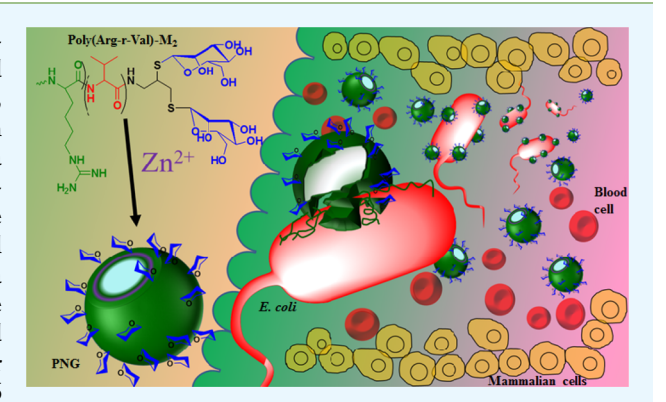
Cite This: ACS Appl. Mater. Interfaces 2019, 11, 33599–33611

Coordination-Assisted Self-Assembled Polypeptide Nanogels to **Selectively Combat Bacterial Infection**

Sudipta Panja,*^{*,†} Rashmi Bharti, Goutam Dey, Nathaniel A. Lynd, and Santanu Chattopadhyay*, Department of the sudiption of

Supporting Information

ABSTRACT: In the present scenario, the invention of bacteriaselective antimicrobial agent comprising negligible toxicity and hemolytic effect is a great challenge. To surmount this challenge, here, a series of polypeptide nanogels (PNGs) have been fabricated by a coordination-assisted self-assembly of a mannose-conjugated antimicrobial polypeptide, poly(arginine-rvaline)-mannose (poly(Arg-r-Val)-M₂), with Zn²⁺ ions. The fabricated PNGs are spherical in shape with a unique structural appearance similar to that of Taxus baccata fruits. PNGs, with a unique structural arrangement and threshold surface charge density, selectively interact with the bacterial membrane and exhibit potent antimicrobial activity, as reflected in their lower minimum inhibitory concentration values (varies from 2 to 16 μ g/mL). PNGs show a remarkably high binding constant, 6.02 \times



105 M⁻¹ (from isothermal titration calorimetry, ITC), with the bacterial membrane which manifests its potent bactericidal effect. PNGs are nontoxic against mammalian and red blood cells as reflected from their higher cell viability and insignificant hemolytic effect. PNGs are taken up by the bacterial membrane and selectively undergo structural deformation (scrutinized by ITC) followed by an exposure of free poly(Arg-r-Val)-M2 molecules. The free poly(Arg-r-Val)-M2 molecules are enforced to lyse the bacterial membrane (visualized by cryo-transmission electron microscopy) followed by the diffusion of the cytoplasmic component out of the membrane which culminates in the final death of the bacterium.

KEYWORDS: antimicrobial polypeptide (AMP), coordination, self-assembly, nanogel, bacterial selectivity, bactericidal effect

INTRODUCTION

In pharmaceutical research, the novel invention of antibiotics had an immense impact on human fertility and morbidity. However, over the last few decades, the emergence of multidrug resistance (MDR) bacteria has remained a major threat to the universal public health. Healing of infectious diseases by prescribing commonly used antibiotics (e.g., ampicillin, chloramphenicol, streptomycin, sulfonamides, tetracyclines, etc.) is being deprived because of the MDR act of the pathogenic bacteria.² Furthermore, the number of approved antibiotics effective against MDR bacteria is decreasing continuously. As per the Diseases Society of America, it is essential to invent at least 10 new antimicrobial agents by the year of 2020.3 Indeed, the days are not too far when currently used antibiotics will be powerless to combat against these infectious diseases.4 Hence, there is an urgent need to invent new antimicrobial agents. Recent, research efforts are mainly concerned with the modification of current antibiotics, searching for new antibiotics, antimicrobial agents⁵⁻⁷ and developing antimicrobial polypeptide (AMP).⁸⁻¹² In contrast to antibiotics, host-defended AMPs

(a vital component of the innate immune system) interact with bacteria by a nonspecific (electrostatic) mechanism which enables them to combat the MDR bacteria efficiently. 14 The cationic moiety of an AMP interacts with the negatively charged phosphate head of lipopolysaccharides (LPSs) which persists on the bacterial cell membrane. Moreover, the hydrophobic moiety of an AMP participates in the interaction with the hydrophobic domain of the membrane. 15 The interaction results in the loss of membrane integrity followed by the diffusion of the cytoplasmic component through the membrane which culminates in the final death of bacteria.

The ideal balance and the spatial arrangement of the hydrophobic and hydrophilic (cationic) moieties enable hostdefended AMPs to selectively mitigate the bacterial infection while remaining nontoxic against the mammalian cell lines. 16 Hence, over the last decade, research efforts have entirely been focused on synthetic AMP mimics. The synthetic AMP mimics

Received: June 10, 2019 Accepted: August 20, 2019 Published: August 20, 2019

[†]McKetta Department of Chemical Engineering, Center for Dynamics and Control of Materials, University of Texas at Austin, Austin, Texas 78712, United States

[‡]Rubber Technology Centre and [§]School of Medical Science and Technology, Indian Institute of Technology Kharagpur, Kharagpur 721302. India

Table 1. Summary of the Composition and Physical and Biological Properties of the Synthesized Polypeptide, Poly(Arg-r-Val)-

					MIC (μg/mL)	
sample	poly(Arg-r-Val)-M ₂	$arginine/valine (mol)^a$	mol. $\operatorname{wt}^b \operatorname{kDa}/B$	zeta $(mV)^c$	EC 8729	SA 29213	$3T3$ cell viability d (%)
	P1	4:1	11.9/1.21	+36± 2.3	2	1-2	18.3 ± 3.1
	P2	3:2	12.5/1.13	+30± 1.4	2	2	32.19 ± 3.6
	P3	2:3	10.6/1.06	$+31\pm\ 1.7$	4-8	2-4	27.02 ± 1.7

^aDetermined by ¹H NMR. ^bMolecular weights were determined by water-phase GPC. ^cSize and zeta potential were determined by DLS. ^dThe cell viability of these samples was tested against 3T3 cells at 100 µg/mL, which is 25 times higher than their MIC values. We have chosen this concentration to have a higher drug safety index of our formulation.

encompass two broadly different categories, that is, synthetic antimicrobial polymers and AMPs. In the case of synthetic antimicrobial polymers, protonated primary ammonium $(-NH_3^+)$, 17 quaternary ammonium $(-NR_3^+)$, 18,19 as well as guanidinium (-NH(CNH)NH₃⁺)²⁰ functionalized polymers, for example, poly(acrylate), poly(imine),21 and biodegradable poly(ester),²² have been reported as essential hydrophilic cationic sources. Cholesterol (an aliphatic hydrocarbon) and smaller aromatic ring-containing polymers have been reported as counterhydrophobic components.²³ Moreover, the multicyclic derivative of the natural product, cholic acid polymer, was also reported as an antimicrobial polymer which adopted local facile amphiphilicity from the repeating units to enhance the interaction with the bacterial membrane.²⁴ For synthetic antimicrobial peptides, the amino acids, lysine, arginine, and histidine, are essentially used as cationic components along with their hydrophobic analogues, leucine, valine, and phenylalanine. 25 Furthermore, the pioneer of AMPs, Gellman's group, has also reported the antimicrobial performance of β -peptides and α/β -peptides. Unfortunately, the exposed cationic charge of synthetic antimicrobial polymers/peptides enforced significant toxicity toward the mammalian cell line and remained highly hemolytic and expressed short circulation half-life in vivo. 16,27-29 Hence, research efforts have continued in search of an improved composition of synthetic AMPs which will show selective antimicrobial effect while remaining nontoxic against mammalian and red blood cells. Recently, there are some reports on supramolecular switchable antibacterial agents that can selectively combat bacterial infections.30,31

To circumvent the aforementioned obstacles and also to enhance the therapeutic performance of synthetic antimicrobial agents, besides the supramolecular antimicrobial agents, nanoformulations of AMPs can also be adopted. It has already been reported that a nanoformulation with a high surface-tovolume ratio results in an intense impact on the biological surface. 32,33 Furthermore, the nanoformulation will assist to preserve most of the interacting functional groups away from nontargeted cell surfaces (by keeping them in the core of the structure) during its administration. Hence, the nanoformulation of the polypeptide will provide a platform in which the cationic moiety will not be exposed and therefore not be toxic. Concurrently, collapsing of a nanoformulation at the bacterial membrane will allow it to selectively kill the bacterium.

Hence, to achieve the proof-of-concept as mentioned above, here, we have synthesized a series of coordination-assisted selfassembled polypeptide nanogels (PNGs) by using poly(Arg-r-Val)-M₂ as a ligand and Zn²⁺ ion as a metal ion source. The AMP, poly(Arg-r-Val)-M2, was synthesized by a random Ncarboxyanhydride (NCA) polymerization of arginine (as a cationic segment) and valine (as a hydrophobic segment) with

different molar ratios (4:1, 3:2, and 2:3). The end group of the finally synthesized polypeptide was functionalized with mannose via thiol-yne click chemistry. The molecular weight, chemical structure, and composition of the synthesized polypeptide were confirmed by gel permeation chromatography (GPC) and nuclear magnetic resonance (NMR) spectroscopy. To minimize the toxicity issue, most of the guanidine groups of poly(Arg-r-Val)-M2 were complexed with Zn²⁺ through coordination-assisted self-assembly. The hydrodynamic diameter, surface zeta potential, as well as the surface and bulk morphologies of the fabricated PNG were examined by dynamic light scattering (DLS), field emission scanning electron microscopy (FESEM), and high-resolution transmission electron microscopy (HRTEM), respectively. The surface composition of the fabricated nanogel was characterized by X-ray photoelectron spectroscopy (XPS). The cell viability (on NIH 3T3 cells) and hemolytic assays (on red blood cells) were performed to evaluate the safety profile of the nanogel. The interaction of the fabricated PNG with the bacterial membrane was visualized by confocal microscopy, FESEM, and cryo-TEM microscopy. The nanogel-induced lysis of the bacterial membrane was visualized by the propidium iodide (PI) assay. The live-dead assay was employed to determine the kinetics of bacterial death at different times (3, 5, and 8 h). The bactericidal effect of pristine poly(Arg-r-Val)-M2 and the fabricated PNG was evaluated by determining the minimum inhibitory concentration (MIC) against Escherichia coli and Staphylococcus aureus. The selective collapse of the PNG at the bacterial membrane was studied (in vitro) by DLS and isothermal titration calorimetry (ITC).

RESULTS AND DISCUSSION

Synthesis of Poly(Arg-r-Val) Copolypeptide. A potent synthetic AMP should contain a definite balance of cationic and hydrophobic segments. Hence, to achieve this balance of cationic and hydrophobic segments, we have synthesized a series of polypeptides by varying the molar ratio of monomers, arginine and valine. The synthesis of monomers, NCA of $N\varepsilon$ trifluoroacetyl-L-lysine (Lys(Tfa)NCA, Figure S1) and NCA of DL-valine (Val NCA, Figure S2), has been done prior to the synthesis of polypeptides. The synthesized polypeptides that exhibit potent antimicrobial performance have an arginine/ valine ratio of 4:1 (sample P1, Table 1), 3:2 (sample P2), and 2:3 (sample P3), respectively. The synthesis of the polypeptides, poly(Arg-r-Val), was performed in a two-step process. The first step involved the synthesis of a statistical copolypeptide, poly(lysine(Tfa)-r-valine), symbolized as poly-(Lys(Tfa)-r-Val) (Scheme S1) by using propargylamine as an initiator followed by the deprotection of the "Tfa" protecting group. The second step comprised the guanidinylation of

lysine's free amine with pyrazole-1-carboxamidine, as mentioned in the Supporting Information (Scheme S2). After the first step, poly(Lys-r-Val) was characterized by ¹H NMR spectroscopy. The spectrum displayed (Figure 1b) signals at

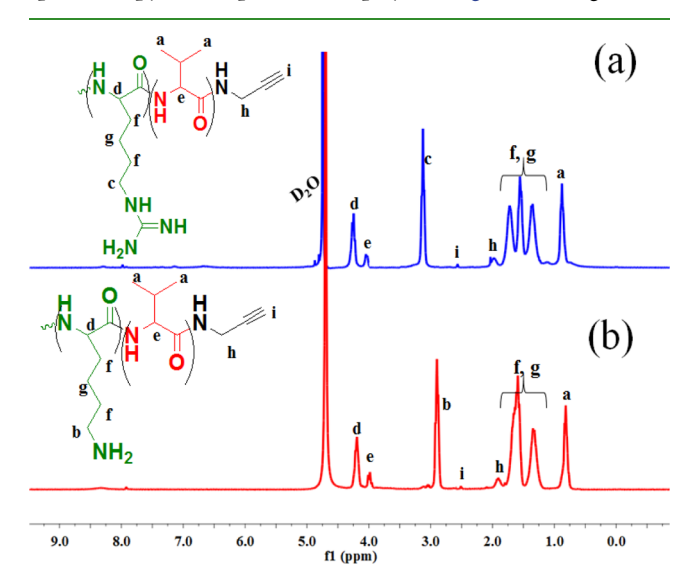


Figure 1. ¹H NMR spectra of (a) poly(Arg-r-Val) and (b) poly(Lys-r-Val) in D₂O (sample P1).

4.23 and 4.00 ppm which were assigned to the methyne group

of lysine $(-NH-C\underline{H}-; d)$ and valine $(-NH-C\underline{H}-; e)$ protons, respectively. The appearance of resonance at 2.80 ppm was attributed to the methylene proton $(-C\underline{H}_2-NH_2; b)$ of the lysine side chain. The signals corresponding to the other side chain methylene protons (-CH₂-; f and g) of lysine appeared as a multiplet in between 1.25 and 1.75 ppm. Furthermore, the ¹H NMR signal of two methyl protons $(-CH_3, a)$ of valine appeared at 0.8 ppm. The appeared signals at 1.82 and 2.41 ppm were assigned to the methylene protons (-CH₂-alkyne; h) and alkyne (alkyne-H; i) proton of the initiator, propargylamine. Hence, the emergence of signals (Figure 1b) corresponding to valine, lysine, as well as propargylamine inferred the successful synthesis of propargylamine-initiated poly(Lys-r-Val). Furthermore, the appearance of ¹³C NMR signals of poly(Lys-r-Val) (Figure S3b) at 173.66 ($\underline{\mathbf{C}}$ =O; g), 53.58 (-NH $\underline{\mathbf{C}}$ HCO; f), 40.90 (- $\underline{\mathbf{C}}$ H₂NH₂; e), 30.49 (-CH₂CH₂CH₂NH₂; d), 27.41 (-CH<u>C</u>H₂CH₂ and $-\underline{C}H(CH_3)_2$; c), 22.29 ($-CH_2\underline{C}H_2CH_2-$; b), and 18.42 $(-\underline{C}H_3; a)$ ppm also supports the structure of poly(Lys-r-Val). In the second step, poly(Lys-r-Val) was renewed to poly(Arg-r-Val) by guanidinylation (Scheme S1). The ¹H NMR of the renewed poly(Arg-r-Val) showed similar characteristic signals (Figure 1a) as for poly(Lys-r-Val) (Figure 1b), except for the shifting of one resonance signal from 2.80 to 3.20 ppm. The shifting of the resonance signal corresponding to the lysine methylene protons $(-C\underline{H}_2-$ NH₂; b, Figure 1b) from 2.80 to 3.20 ppm $(-CH_2-$ NHCONH2; c, Figure 1a) confirmed successful guanidinylation and subsequently the synthesis of poly(Arg-r-Val). In addition, ¹³C NMR of poly(Arg-r-Val) showed (Figure S3a) a unique resonance signal at 156.66 ppm (C=NH; h) for guanidine along with other existing signals, and the Fourier transform infrared (FTIR) spectrum showed a characteristic stretching band at 1542 cm⁻¹ (Figure S4) for the guanidine

functionality. These two conjugative observations also support

the successful synthesis of poly(Arg-r-Val). The molar composition of monomers (valine and arginine) in the synthesized polypeptides (P1, P2, and P3, Table 1) was verified by calculating the integrated area corresponding to the two monomeric protons (Figure S5). For all compositions, the molar ratio of the initiator and the total monomer was held constant. The synthesized polypeptides, P1, P2, and P3 (Table 1), had molecular weights of 11.9 (D = 1.21), 12.5 (D = 1.13), and 10.6 (D = 1.06) kDa, respectively, with a narrower polydispersity (Figure S6).

Synthesis of Thiol Derivative of Mannose (M(OH)₄-SH). Synthesized polypeptides are forthcoming to form selfassembly by involving coordination with metal ions. At this moment, to stabilize the self-assembled structure in a physiological environment, we have chosen mannose as a noncoordinating hydrophilic moiety. The thiol derivative of mannose, M(OH)₄-SH, was synthesized from D(+) mannose through the intermediate synthesis of the acetyl derivative, M(OAc)₄-SH, as described in the Supporting Information The synthesized intermediate, M(OAc)₄-SH, showed a diagnostic ¹H NMR signal (Figure S7) at 5.61 ppm which was attributed to its anomeric proton (O-CH-CH; c) of the six-membered mannose ring. The spectrum also showed a doublet at 2.62 ppm and a multiplet at 2.0 ppm, which were assigned to the thiol proton (-SH; a) and methyl proton (-OCOCH₃; b) of the acetyl protecting group, respectively. The signals corresponding to the other ring protons appeared at 5.25 $(-C\underline{H}(OAc)-; d-f)$ and 4.4 $(-C\underline{H}(OAc)-; g)$ ppm along with the ring peripheral ethylene protons ($-CH-C\underline{H}_2(OAc)$; h) at 4.10 and 4.23 ppm. Hence, all the emerged resonance signals conclude the successful synthesis of the thiol derivative of mannose acetate, M(OAc)₄-SH. The synthesized M(OAc)₄-SH was then subjected to acetyl deprotection with a catalytic amount of NaOMe (Scheme S2). Acetyl-deprotected M-(OH)₄-SH was characterized by ¹H NMR spectroscopy as displayed in Figure S8. The spectrum showed a characteristic anomeric proton signal at 5.21 ppm (O-CH-CH; b). In addition, a number of multiplets appeared in the region from 3.25 to 3.91 ppm which were assigned to the characteristic proton of the six-membered mannose ring (-CH(OH)-; cf). Interestingly, the absence of multiplet signals corresponding to the acetyl protons (at 2.0 ppm) confirmed the successful deprotection of the acetyl group and the subsequent synthesis of $M(OH)_4$ -SH.

Synthesis of Mannose-Conjugated Poly(Arg-r-Val)-M₂. To acquire a nanoformulation with improved colloidal stability, alkyne-terminated polypeptide, poly(Arg-r-Val), was conjugated with the thiol derivative of mannose M(OH)₄-SH by a photoinitiated thiol—yne click reaction (Scheme S1). The mannose-conjugated polypeptide was characterized by ¹H NMR spectroscopy as displayed in Figure 2. The spectrum showed resonance signals at 4.23 (-NH-CH-; c), 3.20 $(CH_2-NH(NH)NH_2; d)$, and 1.25-1.75 ppm $(-CH_2-; e$ g) which were the characteristic signals of the arginine repeating units. The appearance of the signals at 4.00 ppm (-NH-CH-; d) and 0.80 ppm $(-CH_3, a)$ was attributed to the characteristic signals of valine. Furthermore, the appearance of an anomeric proton signal at 5.21 ppm and a multiplet from 3.25 to 3.39 manifested the existence of the mannose moiety. The spectrum of poly(Arg-r-Val)-M₂ demonstrated the disappearance of the signal corresponding to the alkyne proton which would appear at 2.41 ppm (as in Figure 1a). The disappearance of alkyne signals was consistent with the

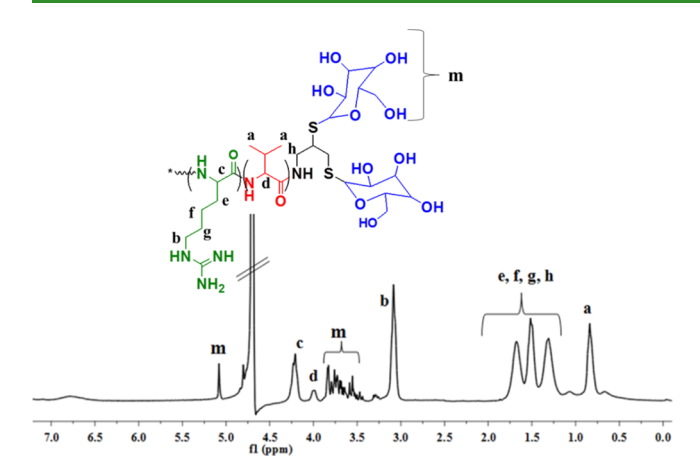


Figure 2. ¹H NMR of the mannose-conjugated polypeptide, poly(Arg-r-Val)-M₂ (sample P1), in D₂O.

conjugation of mannose through the thiol-yne click reaction and the subsequent synthesis of poly(Arg-r-Val)-M2. The synthesized polypeptides showed a positive zeta potential with a slight increase in the value from +31 to +36 mV as we look from sample P3 to P1 (Table 1). The nominal change in the zeta potential can be easily understood by considering the increasing molar ratio of arginine with respect to valine (neutral in charge) as we observe from P3 to P1. The random distribution of hydrophobic valine and hydrophilic arginine results in a completely soluble poly(Arg-r-Val)-M2 which was also supported by the absence of any characteristic peaks in the DLS size profile.

Fabrication of PNG from Poly(Arg-r-Val)-M₂. The synthesized polypeptide, poly(Arg-r-Val)-M2, was fabricated to a smart PNG by coordination-assisted self-assembly.²³ The guanidine groups (-NH(NH)NH₂) of poly(Arg-r-Val)-M₂ functioned as a Lewis base and the metal ions (e.g., Zn²⁺, Fe³⁺, and Cu²⁺) as a counter-Lewis acid. The noncoordinating mannose end groups (-M₂) were dedicated to stabilizing the PNG under physiological conditions. Thus, the formulation of both the Lewis acid and base produced PNG through coordination-assisted self-assembly. Here, polypeptides act as ligands and metal ions as coordination centers (Scheme 1). Although all the three metal ions, Zn²⁺, Fe³⁺, and Cu²⁺, had the proficiency to form PNG, the screening of metal ions was done based on their lower toxicity and efficient antimicrobial activity. The potent antimicrobial activity and minimal toxicity encouraged us to select Zn2+ as the metal ion for the fabrication of PNG.³⁴ PNG was fabricated by varying the molar percentage of Zn2+ from 1.2 to 6% and keeping the numbers of polypeptide molecules as constant. Hence, we fabricated a series of six different PNGs (Table 2) by employing two synthesized polypeptides, P1 and P2 (PNG

from polypeptide P3 has not been reported here), and by varying the molar percent of Zn²⁺ ions. PNGs are symbolized as PNG-n(p) here; "n" indicates the sample number (e.g., n = 1to n = 6) and "p" indicates the polypeptide used (e.g., samples P1 and P2 from Table 1). The formation of the poly(Arg-r-Val)-M₂ and Zn²⁺ complex was successfully confirmed by the shift in the UV absorbance-max from 232 nm (for pristine poly(Arg-r-Val)) to 255 nm (for PNG) with a broadband from 232 to 282 nm (Figure S9). For a particular polypeptide, the particle size of the fabricated PNG showed a growing trend (165-458 nm from PNG-1 to PNG-3 and 190-526 nm from PNG-4 to PNG-5) with an increasing molar percentage of Zn²⁺ ions (from 1.2 to 6%). We hypothesized that with the increasing percentage of Zn2+ ions (for a constant amount of polypeptide), an increasing number of polypeptide molecules come forward and self-assemble together, resulting in a higherorder PNG size.

Unlike size, the positive zeta potential of the PNG decreased from +21 to +15 mV (PNG-1 to PNG-3) and from +18 to +11 mV (PNG-4 to PNG-6) with an increasing molar percent of the Zn²⁺ ion. The decreased surface potential was attributed to the increasing numbers of guanidine moieties involved in the coordination with Zn2+ which resulted in fewer functional groups on the surface of the PNG. The fabricated PNGs are spherical in shape as visualized by FESEM and HRTEM micrographs (Figure 3). The surface morphology (FESEM) of the PNG is very similar to the T. baccata fruit (Figure 3c), which is typically found in southern Europe and Northwest Africa. T. baccata is a well-known biomedical plant from which the famous anticancer drug, paclitaxel, was synthesized. PNG showed several black dots on its structure as visualized by HRTEM (Figure 3b). The black dots were presumed to be because of the persistence of Zn²⁺ ions. The average particle sizes of PNGs obtained from TEM (160 nm for PNG-1 and 180 nm for PNG-4) were in close agreement with the sizes obtained from DLS measurements (165 nm for PNG-1 and 190 nm for PNG-4; Table 2 and Figure S10).

XPS of the Fabricated PNG. The coordination between poly(Arg-r-Val)-M₂ and Zn²⁺, and the surface composition of the PNG, was recognized by high-resolution XPS (HRXPS) (Figure 4). The C 1s HRXPS of the PNG showed (Figure 4a) peaks at 284.5 and 287.9 eV which were assigned to the C-C and C-N/C-O, respectively. The O 1s HRXPS displayed (Figure 4c) peaks for poly(Arg-r-Val)-M2 and PNG at the same binding energy (531.5 eV; O 1s). The result demonstrated the absence of any significant interaction between the "C=O" of the polypeptide and Zn²⁺ during the formation of PNG. However, the N 1s peak for poly(Arg-r-Val) displayed (Figure 4b) a significant shift from 400.2 (N-C) to 402.6 eV $(Zn-N^*-C)$ after the formation of PNG. This observation clearly demonstrated a significant interaction

Scheme 1. Schematic Presentation of the Fabrication of PNG by Coordination-Assisted Self-Assembly of Poly(Arg-r-Val)-M₂



Table 2. Summary of Chemical Composition along with the Physical and Biological Properties of the Fabricated PNG

				MIC (μg/mL)	
^a sample	Zn^{2+} (%)	size (nm) ^b	zeta $(mV)^b$	EC 8729	SA 29213	3T3 cell ^c viability (%)
PNG-1(P1)	1.2	165 ± 3.2	+21 ± 1.9	2-4	2	83.21 ± 3.1
PNG-2(P1)	3	193 ± 1.9	$+18 \pm 1.4$	4	2-4	92.85 ± 3.2
PNG-3(P1)	6	458 ± 2.4	$+15 \pm 2.1$	8	4	96.26 ± 1.7
PNG-4(P2)	1.2	190 ± 3.6	$+18 \pm 1.3$	4	2	86.98 ± 2.6
PNG-5(P2)	3	295 ± 2.7	$+13 \pm 0.9$	4	4	93.23 ± 3.2
PNG-6(P2)	6	526 ± 1.6	$+11 \pm 2.3$	8-16	4-8	91.36 ± 1.9

"PNG-n(p) = "n" indicates the sample number and "p" indicates the polypeptide (Table 1) from which the sample was prepared. MIC of vancomycin is >128 μ g/mL against E. coli and 2 μ g/mL against S. aureus; tested as a positive control. bThe zeta potential and the number average size of the PNG were evaluated from the DLS measurement. bThe cell viability of these samples was examined at 100 μ g/mL. We have chosen this concentration to have a higher drug safety index of our formulation.

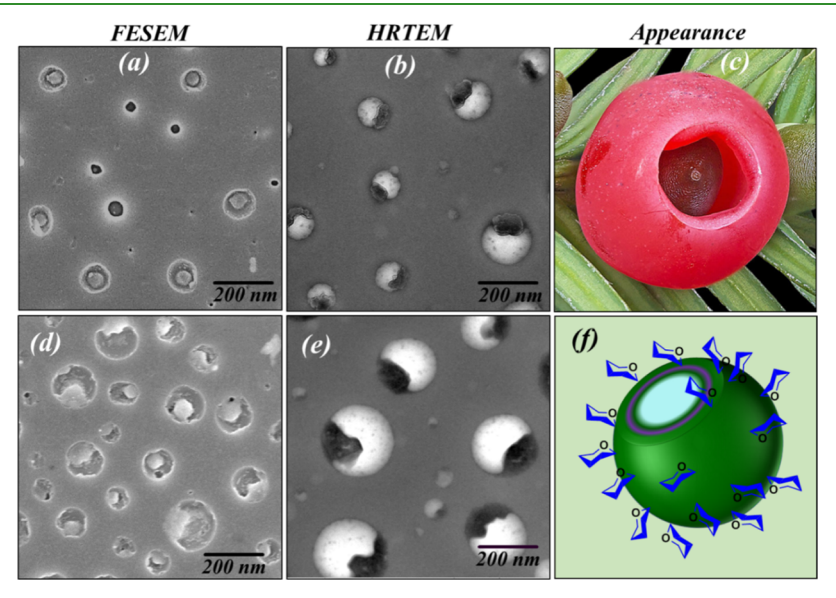


Figure 3. FESEM (a,d) and HRTEM (b,e) images of the fabricated PNG. PNGs appear as the *Taxus baccata* fruit (c) and a schematic presentation of the PNG (f).

(coordination) between guanidine (from poly(Arg-r-Val)) and Zn²⁺ ions. In addition, the Zn 2p HRXPS of PNG (Figure 4d) showed peaks at 1020.5 and 1043.7 eV, which were ascribed to Zn 2P^{3/2} and Zn 2P^{1/2}, respectively. Hence, all the above observations demonstrated the Zn²⁺ ion-mediated coordination-assisted self-assembly of poly(Arg-r-Val)-M₂ that resulted in the formation of PNG.

Therapeutic Performance of Pristine Polypeptide and PNG. The antimicrobial activity of pristine poly(Arg-r-Val)- M_2 and PNG was tested against Gram-positive S. aureus as well as Gram-negative E. coli. All poly(Arg-r-Val)- M_2 showed a lower range of MIC values which typically varies from 1 to 8 μ g/mL (Table 1). In comparison to Gram-negative E. coli, all the synthesized poly(Arg-r-Val)- M_2 showed lower MIC values against Gram-positive S. aureus bacteria. Notably, the evaluated MIC values exhibited a descending trend with increasing arginine content as we look from polypeptide P3 (4 μ g/mL) to P1 (1 μ g/mL) (for S. aureus, Table 1).

This trend was quite expected as higher arginine-containing poly(Arg-r-Val)- M_2 enforced stronger electrostatic as well as hydrogen-bonding interactions with the phosphate head group of the bacterial membrane that resulted in lower MIC. Although absolute arginine-containing polypeptide would provide a stronger interaction with the bacterial membrane, still, they lacked the potent antimicrobial performance. Hence,

to kill the bacterial cells, we need to have an appropriate balance between the cationic (arginine) and hydrophobic (valine) residues.²⁶ Therefore, an appropriate balance of cationic and hydrophobic residues permitted P1 to show superior antimicrobial performance over other polypeptides (P2 and P3, Table 1).

To demonstrate the selectivity, we next examined mammalian cell viability and blood cell viability (hemolytic effect) of poly(Arg-r-Val)-M₂. The cell viability of poly(Arg-r-Val)-M₂ was examined against the mammalian cell line, mouse fibroblast (NIH 3T3) (Figure 5a). The cell viability results revealed that all the synthesized poly(Arg-r-Val)-M2 (P1, P2, and P3) were highly toxic (viability below 35%). Indeed, poly(Arg-r-Val)-M2 was hemolytic against the human red blood cells, erythrocytes (Figure 5b). The concentrations corresponding to the 50% hemolysis (HC50) for samples P1 and P2 were 110 and 133 μ g/mL, respectively (Figure S11). Although the synthesized poly(Arg-r-Val)-M2 showed remarkable antimicrobial performance, they lacked the selectivity for bacteria over mammalian cells. We hypothesized that linear poly(Arg-r-Val)-M2 with fully exposed arginine residues would nonselectively interact with both of the red blood and mammalian cells. The evaluated toxicity results (Figure 5) were also consistent with our hypothesis.^{27,35}

ACS Applied Materials & Interfaces

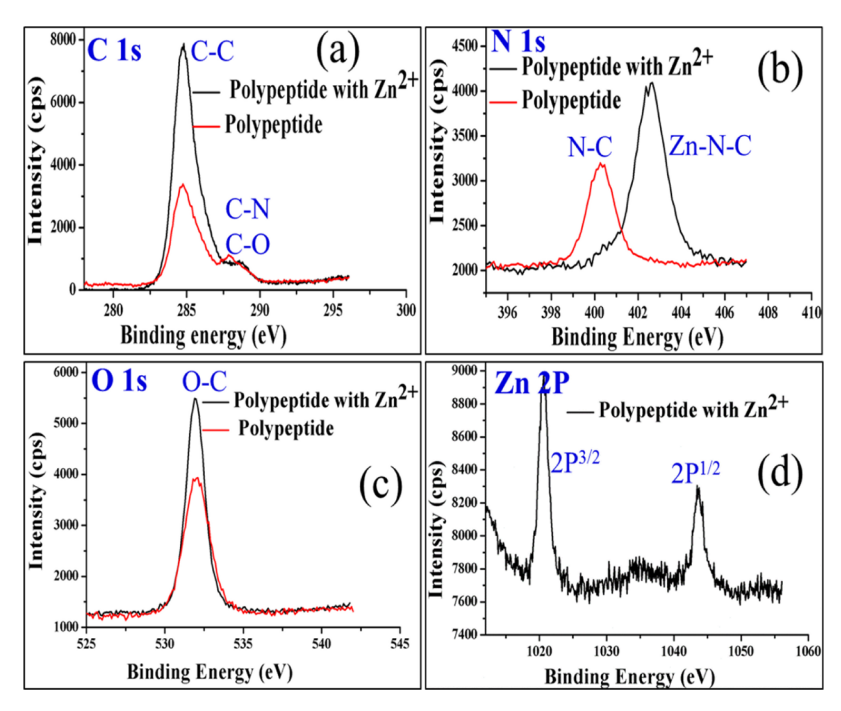


Figure 4. HRXPS of (a) C 1s, (b) N 1s, (c) O 1s, and (d) Zn 2p spectra collected from the polypeptide (sample P1) and the fabricated PNG (sample PNG-1).

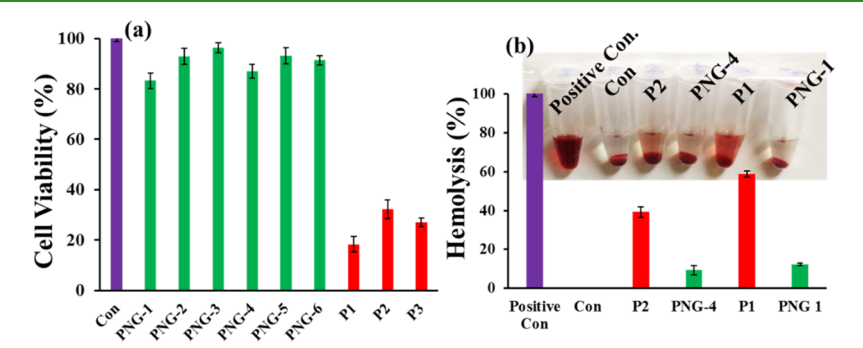


Figure 5. (a) Cell viability assay (against 3T3 cell line) and (b) hemolytic assay of the polypeptide and PNG at $100 \,\mu\text{g/mL}$. We have chosen this concentration to have a drug safety profile of our formulation. The concentration ($100 \,\mu\text{g/mL}$) is 25 times higher than the average MIC of the samples.

To improve antimicrobial selectivity, poly(Arg-r-Val)-M₂ was subjected to PNG fabrication. During PNG fabrication, most of the arginine residues were pulled into the core of the structure, with the terminal mannose residues (M) being expressed on the corona (Scheme 1). Now, to investigate the therapeutic potential of PNG, we tested cell viability, hemolysis, and antimicrobial activity. Interestingly, PNGs appeared to be nontoxic (cell viability above 80%, Figure 5a and Table S1) with insignificant hemolytic activity (less than 13% @ 100 μ g/mL, Figure 5b and Table S1). The HC50 values for the samples PNG-1 and PNG-4 were evaluated as 798 and 961 μ g/mL, respectively (Figure S11). Adequately, the PNGs were selectively noxious toward bacterial cell, and their MIC values ranged from 2 to 16 μ g/mL (Table 2, E. coli). The obtained MICs of PNG were significantly lower than the traditionally used antibiotic, vancomycin (>128 µg/mL against E. coli tested as a positive control). PNG exhibited a decreasing order of MIC with decreasing percentage of Zn²⁺ content (from 6 to 1.2%) as we look (Table 2) from PNG-3 to PNG-1 (fabricated from P1) and from PNG-6 to PNG-4 (fabricated from P2). A similar trend of MIC was observed (Table S2)

against the resistant strain of Gram-negative $E.\ coli$ and Gram-positive methicillin-resistant Staphylococcus aureus (MRSA). We hypothesized that the structure of PNG is selectively disrupted on the bacterial membrane and enables the free poly(Arg-r-Val)- M_2 chains to interact with and spontaneously kill the bacteria. However, PNG remained almost intact against both the mammalian cells and red blood cells, as reflected from the hemolysis and cell viability results. It is worth to mention that Zn^{2+} on its own also has antimicrobial activity. The electrostatic interaction (between Zn^{2+} and the bacterial cell membrane) and the production of reactive oxygen species are the two underlying mechanisms of killing the bacterial cell. However, the existence of Zn^{2+} ions in our PNG formulation was nominal (max. 6% mol with respect to poly(Arg-r-Val)- M_2) which resulted in an insignificant synergistic effect.

The stability of PNGs in the presence of fetal bovine serum (FBS) (10% to mimic the traditional cell culture) was studied by DLS over a time period of 24 h. We used PNG-1 and PNG-3 (Table 2) to evaluate their stability in FBS. The hydrodynamic diameter (Figure S12) of the nanomaterial PNG-3 with FBS remained the same over the period of 24 h.

ACS Applied Materials & Interfaces

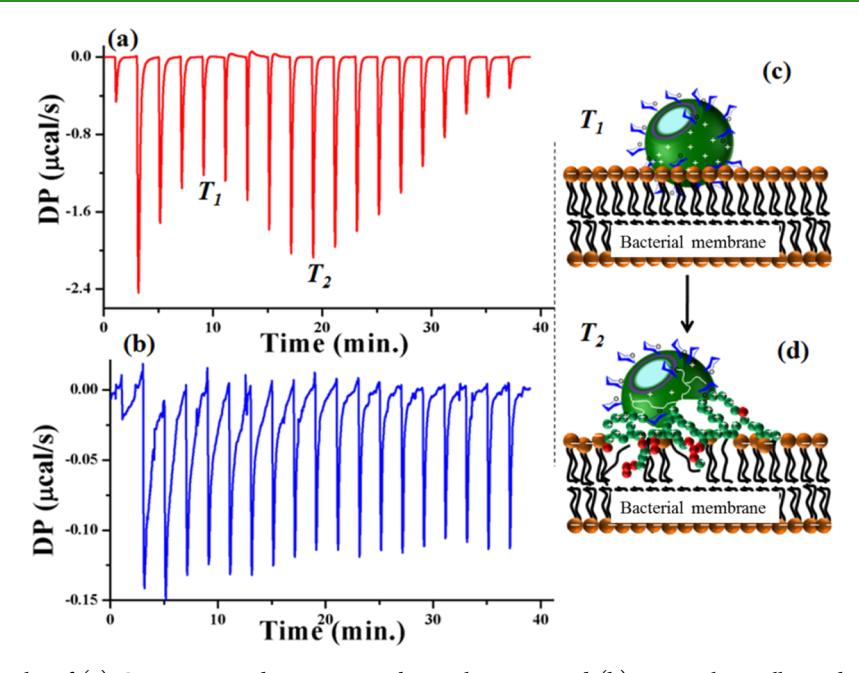


Figure 6. ITC titration results of (a) Gram-negative bacteria mimicking a liposome and (b) mammalian cell membrane mimicking a liposome against PNG. A schematic presentation of PNG deformation on the bacterial membrane at the fifth (T_1, c) and tenth injection (T_2, d) points.

Table 3. Summary of Different Thermodynamic Parameters Evaluated from ITC Experiments

compor	nent ^a	ΔG^b (kcal/mol)	ΔH^b (kcal/mol)	$-T\Delta S^b$ (kcal/mol)	$K_a^b (M^{-1})$
PNG	bacterial cell	-7.89	-12.90	5.04	6.02×10^5
	mammalian cell	ND	ND	ND	ND
poly(Arg-r-Val)-M ₂	bacterial cell	-8.26	-10.70	2.47	1.13×10^{6}
	mammalian cell	-6.00	-10.90	4.86	2.84×10^{4}

"Bacterial cell OM = liposome prepared by POPC and LPS at a ratio of 4:1 and mammalian cell = liposome prepared by POPC only. ${}^{b}K_{a}$ = binding constant. ND = not able to determine.

However, PNG-1 showed a minor increase in hydrodynamic size (163–186 nm) after 6 h of incubation with the serum. Thereafter, its size remained constant over the period of next 24 h. The nominal increase of size might be attributed to the fractional adsorption of serum protein onto the surface of the particle. However, the structure of PNG-1 remained intact as the increased size (186 nm) was maintained up to 24 h. Hence, the structure of the PNG nanomaterials remained intact in the presence of FBS.

Now, to understand the bacteria-killing kinetics for both the pristine poly(Arg-r-Val)-M₂ and PNG, we performed the livedead assay at three different times (3, 5, and 8 h) against E. coli. The live-dead assay assists us to differentiate the dead cells from live cells. On the basis of this assay, the live cell takes calcein-AM (green) and the dead cell takes ethidium homodimer (red), as visualized by fluorescence microscopy. Both poly(Arg-r-Val)-M2 and PNG showed increasing numbers of dead cell populations with time (Figure S13). However, in comparison to PNG, pristine poly(Arg-r-Val)-M₂treated well plate showed a large number of dead cell population at all time frames. Hence, pristine poly(Arg-r-Val)-M₂ was hasty to kill the bacterial cells. PNGs were active toward both the Gram-positive (S. aureus) and Gram negative (E. coli) bacteria, and it has already been realized that E. coli are highly resistant because of the existence of their outer membrane (OM). Hence, to gain a superior understanding of PNG and bacterial interaction, we selected Gram-negative E. coli to pursue our further studies.

Bacteria-Selective Antimicrobial Performance of PNG. Pristine poly(Arg-r-Val)-M2 showed remarkable antimicrobial performance. However, significant toxicity (Table 1) toward the mammalian cell line restricted their implementation to antimicrobial therapy. On the contrary, the fabricated PNGs exhibited potent antimicrobial activity without significant nonspecific toxicity against the mammalian cells. To better understand the bacteria-selective antimicrobial performance of the PNG and the toxicity of pristine poly(Arg-r-Val)-M2 against the mammalian cells, we have evaluated the thermodynamics of membrane-PNG interactions by ITC (Figure 6) using a liposome model.³⁷ The liposome prepared from the lipid, 1-palmitoyl-2-oleoyl-sn-glycero-3-phosphocholine (POPC), was used to mimic the mammalian cell membrane, and a combination of POPC and LPS was used to mimic the OM of Gram-negative bacteria (e.g., E. coli) (described in the Supporting Information). Pristine poly(Argr-Val)-M₂ showed (Table 3) a negative free energy of binding (Figure S14) for both the Gram-negative bacteria and mammalian cell membrane mimicking liposomes with a binding constant (K_a) of 1.13×10^6 and 2.84×10^4 M⁻¹,

Poly(Arg-r-Val)- M_2 has a huge number of randomly distributed positively charged guanidine functional groups that nonspecifically interact with both mammalian cells as well as bacterial OMs, which is a consequence of its higher K_a value. In comparison with mammalian cells, the interaction of poly(Arg-r-Val)- M_2 with E. coli was marginally stronger, as

reflected in its higher K_a value. We hypothesized that the higher density of the negative charge on the OM of the Gramnegative bacteria was because of its stronger electrostatic interaction with the positively charged poly(Arg-r-Val)-M₂. Additionally, the interaction between poly(Arg-r-Val)-M₂ and mammalian cells was not negligible $(K_a = 2.84 \times 10^4 \text{ M}^{-1})$ Figure S14a) as it exhibited significant toxicity toward mammalian cells (Figure 5a). Hence, to improve the therapeutic performance of poly(Arg-r-Val)-M2, we fabricated PNG by coordination-assisted self-assembly with Zn²⁺ ions. PNG showed stronger binding with the bacterial OM, as reflected in its negative free-energy change, $\Delta G = -7.89 \text{ kcal/}$ mol and $K_a = 6.02 \times 10^5 \,\mathrm{M}^{-1}$ (Table 3). However, the binding event between the PNG and mammalian cell membrane imposed no significant free-energy change (Figure 5b), which is consistent with their associated low toxicity. These phenomena can be effortlessly understood by considering the structural rearrangement that occurs during the PNG fabrication (from poly(Arg-r-Val)-M2). During the formation of PNG, most of the positively charged guanidine moieties were pulled into the core, whereas mannose (M2) faced outward the corona (Scheme 1), which resulted in an enormous reduction in surface charge density. The reduction in the surface zeta potential (after PNG formation) from +36 mV (polypeptide, P1, Table 1) to +21 mV (PNG-1(P1), Table 2) was consistent with the above phenomena.

At this moment, PNG with a unique nanostructure and threshold surface charge density selectively experienced structural disruption at the bacterial OM. The increase in the hydrodynamic diameter (Figure S14a) from 193 to 512 nm (sample PNG-2) with the concentration of E. coli mimicking liposome also supported the structural disruption process. Structural disruption followed by neutralization of the exposed charge from PNG resulted in aggregation followed by an increase in the effective hydrodynamic diameter (193-512 nm). Indeed, PNGs were inert against mammalian cells with no significant change in the hydrodynamic size being evident (Figure S14b). The interaction of PNG with bacterial OM was further investigated by considering the nature of the ITC curve which displayed two sets of transitions (Figure 6a). Interestingly, the heat release gradually dropped off up to the fifth injection point (T1, Figure 6a) and again started to increase just after the seventh injection point, reaching a maximum at the 10th injection point $(T_2, Figure 6a)$ followed by slow convergence to equilibrium. We hypothesized that the first transition (T₁) was because of the initial involvement of PNG with the negatively charged bacterial membrane via electrostatic interactions (Figure 6c). Thereafter, PNG undergoes structural disruption at the bacterial surface followed by the exposure of an enormous amount of positive charge (Figure 6d). The second transition (T2; started at the 10th injection) was caused by the interaction of an additional exposed charge (after PNG disruption) with the bacterial OM. An identical ITC experiment of bacterial suspension against PNG showed a similar thermogram (Figure S15) as with bacteria mimicking the liposome model. The first transition (T_1) happened at a very short period of time which implied the faster involvement of PNG with the bacterial cell. Micrometersized bacteria with enormous surface charge rapidly interacted with nanometer-sized (nm scale) PNG which caused its shorter transition time. The second transition (T_2) , that is, the unfolding of the PNG structure with the increasing concentration of bacteria, was identical with the liposome

model. As PNGs were formed by the coordination-assisted self-assembly of poly(Arg-r-Val)-M2 with Zn2+, at the bacterial OM, poly(Arg-r-Val)-M₂ (from PNG) should experience a competitive binding interaction between the bacterial OM and Zn²⁺ ions (from PNG). Presumably, the stronger electrostatic binding interaction of poly(Arg-r-Val)-M2 (from PNG) with the bacterial OM constrained the PNG to undergo a structural deformation. On the contrary, the electrostatic binding interaction between poly(Arg-r-Val)-M2 (from PNG) and the mammalian cell membrane was not strong enough to show any structural deformation causing the PNG to appear as nontoxic.

Mechanism of Bacteria Killing. To further understand the interaction of bacterial cells with PNG, rhodamine B (RhB; red dye) was loaded into the PNG.^{38–40} Meanwhile, to get a prominent contrast, bacterial DNA was counterstained by Sytox green. Confocal images were captured at 0.25 and 1 h, as displayed in Figure 7. The appearance of red fluorescence at

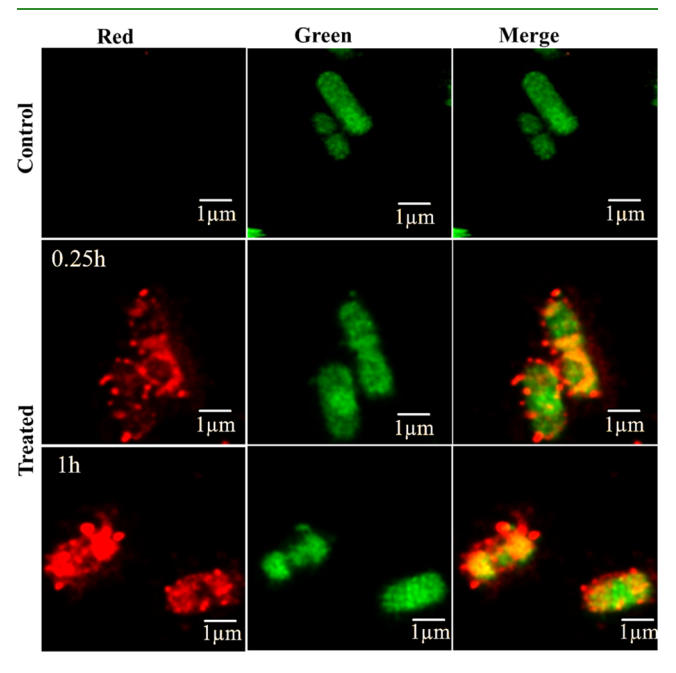


Figure 7. Confocal microscopic image of RhB-encapsulated PNGtreated E. coli at the time intervals of 0.25 and 1 h; DNA of the bacterial cell was stained by Sytox green.

the bacterial membrane implied a significant interaction of PNG with the bacterial membrane. The electrostatic attraction of positively charged PNG toward the negatively charged bacterial membrane was the origin of this interaction.⁴¹ Furthermore, PNG uptake showed an increasing trend (intensity of red fluorescence at the membrane) with time (from 0.25 to 1 h). Hence, the bacterial membrane was dynamic and demonstrated a time-dependent uptake of PNG.

To recognize the underlying mechanism of bacterial cell death, PNG-treated and untreated bacteria were visualized under cryo-TEM (Figure 8). The control experiment (untreated) showed a rod-shaped E. coli with a clear visualization (Figure 8a,b) of two intact membranes (outer and inner). However, the PNG-treated *E. coli* induced (Figure 8d-e) significant damage to the OM. Furthermore, the effect was prolonged up to the inner membrane. In addition, some parts (green arrow) of the membrane showed blebbing and budding. This blebbing is quite clear on the FESEM image (Figure 8f, green arrow) of PNG-treated E. coli. The entropy-favorable

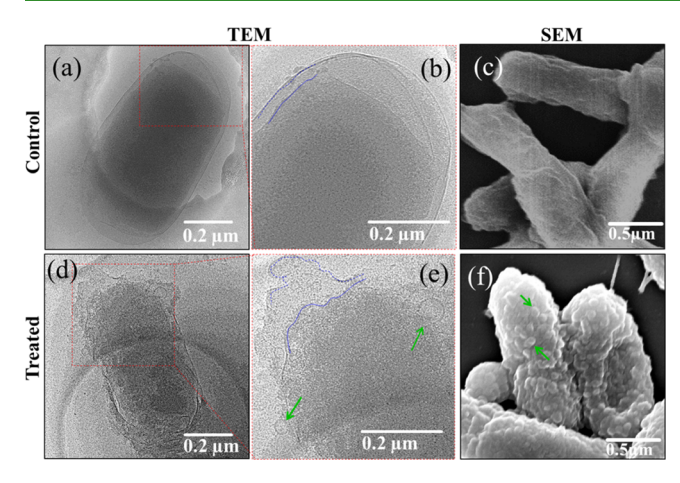


Figure 8. Cryo-TEM images of control (a) and PNG-treated (d) E. coli. The images (b,e) are the zoomed areas (red-marked) of (a,d). The inner membrane and OM of E. coli are highlighted (b,e) by solid and dotted blue lines to guide the eye. FESEM images of control (c) and PNG-treated (f) E. coli.

electrostatic attraction of poly(Arg-r-Val)-M₂ (from PNG) to the bacterial membrane is proposed to be the cause of blebbing and budding followed by a permanent damage of the membrane. 42 Moreover, poly(Arg-r-Val)-M2 (from PNG) with arginine and hydrophobic valine moieties enforced the organization of the bulky lipid head groups of the membrane which resulted in the destabilization of the membrane by producing a saddle splay membrane curvature. Furthermore, the appearance of red fluorescence (from PI assay, Figure S16) after 3 h of PNG-treated bacterial cell indicated the adequate rupture of the bacterial membrane. Considering all the above observations, we confirmed that the interaction of PNG with the bacterial membrane resulted in the lysis followed by the diffusion of most of the cytoplasmic components through the membrane, leading to bacterial death.

CONCLUSIONS

In conclusion, we have synthesized a series of mannoseconjugated statistical copolypeptides, poly(Arg-r-Val)-M2, by NCA polymerization followed by thiol-yne click functionalization. Poly(Arg-r-Val)-M2 undergoes coordination-assisted self-assembly in the presence of Zn²⁺ ions, as reflected from their UV-vis absorption band shift (from 232 to 283 nm) and N 1s peak (from HRXPS) shift from 400.2 (N-C) to 402.6 eV $(Zn-N^*-C)$. The self-assembly of poly(Arg-r-Val)-M₂ resulted in the formation of PNG which had a unique appearance similar to the T. baccata fruit, as visualized in both the HRTEM and FESEM images. The fabricated PNGs were potent to show the bactericidal effect as revealed from their lower range of MIC values $(2-16 \mu g/mL)$ which were significantly lower than the traditionally used antibiotic, vancomycin (>128 μg/mL; E. coli). Noteworthily, PNG exhibited higher cell viability (above 80%) against mammalian cells with a negligible hemolytic effect. The stronger electrostatic binding interaction ($K_a = 6.02 \times 105 \text{ M}^{-1}$) with the bacterial OM constrained the PNG to selectively undergo structural deformation. On the contrary, the binding interaction between the PNG and the mammalian cell membrane was insignificant which offered PNG to appear as nontoxic. PNGs were taken up by the bacterial membrane (visualized by confocal microscopy), resulting in the structural

disruption and discharge of free poly(Arg-r-Val)-M2 molecules. The exhaustive interaction of free poly(Arg-r-Val)-M2 molecules with the bacterial membrane resulted in budding and blebbing on the bacterial membrane followed by the complete lysis of the membrane. The membrane lysis enforced the bacteria to diffuse the cytoplasmic components throughout the membrane, resulting in the final death of the bacterial cells.

Hence, here, we introduced a polypeptide-based unique nanostructure which exhibited a superior bacterial selective therapeutic performance in comparison to the pristine polypeptide. Furthermore, the self-assembly approach introduced a new therapeutic window, where the toxic synthetic polypeptides which are suffering from clinical approval can be formulated to nontoxic nanostructures without compromising the antimicrobial activity.

EXPERIMENTAL SECTION

Materials. $N\varepsilon$ -Trifluoroacetyl-L-lysine (Lys(Tfa)), valine (Val), triphosgene, propargylamine, 1H-pyrazole-1-carboxamidine hydrochloride, D(+) mannose, 2,2-dimethoxy-2-phenylacetophenone (DMPA), the hydrogen form of Amberlite IR120, HBr in acetic acid (33%), and zinc nitrate hexahydrate (Zn(NO₃)₂·6H₂O) were purchased from Sigma-Aldrich, USA. Sodium bicarbonate (NaHCO₃), potassium carbonate (K₂CO₃), magnesium sulfate (MgSO₄), sodium thiosulfate (Na₂S₂O₃), thiourea (NH₂CSNH₂), sodium metabisulfite (Na₂S₂O₅), and sodium methoxide (NaOMe) were procured from Merck Chemicals, Mumbai, India. The solvents, anhydrous ethyl acetate, hexane, tetrahydrofuran, dimethyl sulfoxide (DMSO), dichloromethane, and methanol (MeOH), were purchased from Sigma-Aldrich, USA. Other common solvents, diethyl ether, acetic anhydride, and acetone, were purchased from Merck Chemicals, Mumbai, India. The cellulose acetate dialysis tube (cut off 3.5 kDa) was purchased from SnakeSkin Thermo Scientific, India.

Synthesis of Propargylamine-Initiated Poly(Lys(Tfa)-r-Val). The random copolymer of lysine and valine was synthesized by NCA polymerization (Scheme S1) of the respective monomers (mentioned in the Supporting Information) using propargylamine as an initiator. The random polymerization of lysine and valine was performed at three different molar compositions of lysine and valine, such as 4:1, 3:2, and 2:3, for a constant equivalent (1 equiv) of the initiator, propargylamine (Table 1). The required amounts of NCA of lysine and valine were taken in a dry round-bottom flask (RBF) under N2 atmosphere. Dry dimethylformamide (DMF) was added into the RBF (conc. 1 g/10 mL of DMF) under an ice-cooled condition followed by the addition of a required amount of propargylamine. The RBF was then brought to room temperature and allowed to stir for 24 h. The completion of polymerization was inspected by recording the FTIR of a small aliquot of the reaction mixture. After completion, the reaction mixture was precipitated into excess diethyl ether and centrifuged (at 10k rcf for 10 min) to collect the precipitated polymer. The precipitated polymer was dried overnight in a vacuum oven prior to characterization.

The deprotection of the "Tfa" group was performed in an aqueous solution of K₂CO₃. In brief, 0.5 g of the synthesized polymer was dispersed into a 50 mL of water and methanol mixture (2:3 by volume). The suspension was heated to reflux followed by the addition of 0.3 g solid K₂CO₃. After an overnight reflux, the reaction mixture was cooled down to room temperature, and the volume of the mixture was reduced to one-third of its initial volume. The reaction mixture was then purified by dialysis against water (4 days). The purified polymer was freeze-dried and characterized by NMR.

Synthesis of Poly(Arg-r-Val) Copolymer from Poly(Lys-r-Val). The lysine moiety of the random copolymer was converted to arginine (Arg) by guanidization (Scheme S1) with 1H-pyrazole-1carboxamidine hydrochloride. Poly(Lys-r-Val) (1 g) was dissolved into 20 mL of dry DMSO under N2 atmosphere. Lysine's amine activating agent, N,N-diisopropylethylamine, was added (5 equiv with respect to amine) into the DMSO-dissolved polypeptide solution and stirred for 15 min. The reaction mixture was heated to 100 °C followed by the addition of DMSO-dissolved 1H-pyrazole-1carboxamidine hydrochloride (1.5 equiv with respect to amine). The reaction was continued overnight under N2 atmosphere. The reaction mixture was purified by dialyzing against water (4 days). Finally, poly(Arg-r-Val) was freeze-dried and characterized by NMR spectroscopy and GPC.

Synthesis of the Thiol Derivative of Mannose (M(OH)₄-SH). To synthesize the thiol derivative of mannose, the acetyl group of M(OAc)₄-SH (synthesis has been mentioned in the Supporting Information)^{28,29} was deprotected by NaOMe (Scheme S2). was deprotected by NaOMe (Scheme S2). M(OAc)₄-SH (1 g, 2.74 mM) was dissolved into 20 mL of dry MeOH followed by N2 purging for the next 15 min to remove the dissolved O2. NaOMe in MeOH (2 mL, 1 M) solution was injected into the reaction mixture and stirred for 12 h at room temperature. The reaction mixture was diluted with excess MeOH and neutralized by the hydrogen form of Amberlite IR120. The final solution was filtered and concentrated under a rotary evaporator. The dry product was characterized by NMR spectroscopy.

Synthesis of Mannose-Conjugated Poly(Arg-r-Val)-M2 by Thiol-Yne Click Reaction. An alkyne-terminated random copolymer, poly(Arg-r-Val), was conjugated with mannose via the thiol-yne click reaction (Scheme S1). Poly(Arg-r-Val) (1 equiv) and M(OH)₄-SH (2.5 equiv) were dissolved in MeOH (concentration: 1 g/20 mL) and allowed to purge with N2 (15 min). The MeOH-dissolved initiator, DMPA, was injected into the reaction mixture, and the N2 purging was continued for another 15 min. The whole reaction flask was then subjected to UV light (365 nm) in a dark place with continuous stirring for the next 4 h at room temperature. After the completion, the reaction mixture was diluted with water and subjected to dialysis (4 days) against water. The purified polymer was lyophilized to get a white solid and characterized by NMR spectroscopy.

Fabrication of Coordination-Assisted Self-Assembled PNG from Poly(Arg-r-Val)-M₂. The self-assembly of the synthesized polymer was achieved by using a metal ion as a coordination center and guanidine (from the arginine moiety) as a ligand (Scheme 1). The preparation technique is partly similar with our previously reported nanostructure. 43 In brief, poly(Arg-r-Val)-M2 was dissolved in phosphate-buffered saline (PBS) at a concentration of 50 mg/mL, and a solution of the metal salt, Zn(NO₃)₂·6H₂O (10 mM), was prepared separately. The polymer solution (200 μ L) was taken in an Eppendorf safe-lock tube followed by a controlled addition of salt solution under sonication. The mixture was centrifuged (10 min @ 10k rcf) and the supernatant was decanted off to remove the trace amount of unbound metal ions. The precipitate was redispersed in a required volume of PBS to maintain a 10 mg/mL final polymer concentration. For a constant amount of poly(Arg-r-Val)-M2 solution, different volumes of metal ion solution (10 mM) were added to get a library of self-assembled nanostructures (Table 2) with various molar percentages of metal ion content. The fabricated PNG was characterized by DLS, FESEM, and HRTEM.

Minimum Inhibition Concentration. The MIC of both of the pristine polypeptide and fabricated PNGs were determined by a broth microdilution method using two bacterial ATCC strains that are sensitive to most of the commonly used antibiotics. 44-47 Gramnegative E. coli (ATCC 8739) and Gram-positive S. aureus (ATCC 29213) microbial cells were subcultured followed by homogenization of the mid-log phase (after 4 h) of microbial cells. The optical density (at 600 nm) of the microbial cell-loaded test plate was measured to get a final cell concentration of 5×10^6 CFU/mL by appropriate dilution. Mueller-Hinton broth was taken into a 96-well plate followed by the addition of a stock solution of PNG in a serial dilution manner. Eventually, the bacterial culture was added to each well. The culture plate was then incubated for 18 h at 37 °C under aerobic condition. The wells without nanogel and with inoculums were maintained to have a control. The wells with vancomycin-treated cells were maintained to have a positive control. MICs of the samples were determined as the lowest concentration that inhibited more than 90% of cell growth. Two independent experiments with three replicates of each were performed, and the results are presented as mean. The MIC values for the samples P1, P2, P3, PNG-1, PNG-3, PNG-4, and PNG-6 were evaluated against the resistant strain of Gram-positive MRSA and Gram-negative E. Coli by following the above-mentioned protocol. The results are presented in Table S2.

3-(4,5-Dimethylthiazol-2-yl)-2,5-diphenyltetrazolium Bromide Assay. The cell viability of the pristine polypeptide and the fabricated PNG was tested against the widely used mammalian cell line, NIH 3T3 (mouse fibroblast). The 3T3 cells were seeded into six-well plates in 2 mL growth media containing Dulbecco's modified Eagle's medium suspended with 10% FBS. The cells were then allowed to grow for the next 2 days until 80% confluent. In the next step, the grown cells were seeded into a 96-well plate at the concentration of 5×10^3 cells per well with the culture medium. The culture plate was incubated at 37 °C with 5% CO2 humidified atmosphere for 24 h. The sample (polypeptides and PNGs) solution was prepared by dissolving into the growth medium at two different concentrations, 100 and 200 μ g/mL. The medium in each well was replaced with 100 μ L of sample solutions. The culture plates were then incubated for 24 h at 37 °C with 5% CO₂ atmosphere. A control well was maintained without the treatment of the sample solution. After the incubation time, the medium in each well was replaced with 3-(4,5-dimethylthiazol-2-yl)-2,5-diphenyltetrazolium bromide (MTT) solution (1 mg/mL) and allowed to incubate for an additional 4 h. The cultured supernatant was then replaced with 100 μ L of DMSO and allowed to dissolve all the formazan crystals. Finally, the absorbance of each well was collected at 590 nm using a microplate reader (Bio-Rad, Hercules, CA). Two sets of MTT experiment were performed for two different concentrations (100 and 200 $\mu g/mL$), and each set was maintained in triplicate. The average value of the result with ±SD is presented here. The cell viability of these samples was tested against 3T3 cells at 100 and 200 μ g/mL, which are about 25 and 50 times higher than their MIC values, respectively. We have chosen these concentrations to have a drug safety profile of our formulation. The results obtained from the 200 $\mu g/mL$ sample concentration are mentioned in the Supporting Information (Figure

Hemolytic Assay. The blood sample was collected from an adult healthy donor in a BD Vacutainer blood collection tube. The collected sample was freeze-stored for 30 min (at 4 °C) prior to use. The erythrocytes were separated by centrifuging the sample for 10 min at 1000 rpm using SiColl. The sample was then washed thrice with chilled PBS and a 5% (v/v) stock solution was prepared by adjusting the concentration with chilled PBS. Thereafter, 100 μ L of each test sample (concentration 100 μ g/mL) was separately mixed with 100 μ L of erythrocyte cells in a 1 mL microcentrifuge tube (sterilized). The mixture of the test sample with erythrocytes was then subjected to incubation for 2 h at 37 °C on a horizontal shaker at 150 rpm. After the allowed time, the mixture was centrifuged at 1000 rpm for 10 min to spin down the intact erythrocytes. The supernatant (50 μ L) was deliberately transferred into a 96-well microplate followed by half-dilution with 50 μ L of PBS. The hemolytic activity of the test samples was evaluated by taking the absorbance of the supernatant at 540 nm using a microplate reader (Bio-Rad, Hercules, CA). Erythrocytes with PBS solution and erythrocytes with 0.01% Triton X-100 were maintained as a negative and positive control, respectively. The percentage of hemolysis was calculated by the following equation (eq 1)

Hemolysis (%) =
$$\frac{(A_{\rm S} - A_{\rm NC})}{(A_{\rm PC} - A_{\rm NC})} \times 100$$
 (1)

Here, A_{S} , A_{NC} , and A_{PC} represent the absorbance of the sample, negative control (PBS), and positive control (Triton X-100), respectively. The hemolysis (%) of each sample was evaluated at various concentrations (100, 200, 400, 800, and 1000 μ g/mL) by using the same protocol. The concentration corresponding to the 50% hemolysis was designated as HC50.

Pl Assay. For PI assay, a stock solution of Gram-negative E. coli (ATCC 8739) at the concentration of 5×10^6 CFU/mL was prepared in an identical way as mentioned in the MIC protocol. The bacterial cells were then incubated with 100 $\mu g/mL$ sample (PNG) for 3 h at 37 °C at a shaking (horizontal) speed of 250 rpm. Thereafter, the PI solution (2 μ M) was added into the bacterial culture solution and incubated for another 0.5 h in the dark. The sample was then placed on a glass slide and the image was captured by placing the slide on the fluorescence microscope (Carl Zeiss, Oberkochen, Germany).

Live—Dead Assay. The live—dead assay of bacterial cells was performed with the polypeptide and PNG. Hence, to do this, we have cultured *E. coli* (ATCC 8739) cells in an identical way as mentioned in the MIC protocol and maintained the cell concentration of 5 × 10⁶ CFU/mL. The polypeptides (P1, P2, and P3) and PNG (PNG-1 to PNG-6) were incubated with bacterial cells at the dose of their MIC. We have varied the incubation time as 3, 5, and 8 h for each sample to have a killing kinetics. After the desired time, the corresponding cells were washed with PBS and stained with live—dead stain, ethidium homodimer and calcein AM, and retained for 15 min under dark. The stained bacterial cells were then washed with PBS thrice followed by mounting on glass slides to capture the fluorescence image of the live (green) and dead (red) cells. The numbers of live and dead cells were counted by using ImageJ software, and the average of three results is presented here along with their representative images.

Nanogel and Bacterial Membrane Interaction. Confocal. For optical microscopy, RhB was encapsulated during the preparation of PNG from the polypeptide.⁴⁹ Excess RhB was removed by dialysis (cutoff M_n 3.5 kDa, cellulose acetate). The RhB-loaded nanogel at their MIC concentration was incubated (as like MIC protocol) with E. coli (5 \times 10⁶ CFU mL⁻¹) at 37 °C for 0.25 and 1 h. Sytox green was employed to stain the DNA of E. coli. After 15 min of incubation, the bacterial cells were centrifuged and washed with PBS (thrice). Formaldehyde (2.5%) was used to fix the cells, followed by washing with PBS (twice), and finally, resuspended. A poly-L-lysine-coated glass slide was used to spot the cell. The spotted slide was incubated at room temperature for few hours and then washed with PBS to wash out the nonadhering cells. Finally, the images were captured under a confocal microscope. The details of the FESEM (following Liu et al.)²³ and cryo-TEM sample preparation (following Chen et al.)⁵⁰ are mentioned in the Supporting Information.

Isothermal Titration Calorimetry. The thermodynamic parameters for the binding event between the bacterial membrane and PNG have been evaluated by ITC using a MicroCal Malvern instrument.³⁷ To demonstrate the competitive interaction of the polypeptide and PNG toward the membranes of mammalian and bacterial (Gram-negative) cells, two types of liposomes were prepared by using lipids, namely, POPC and LPS. The lipid POPC was used to mimic the mammalian cell membrane, and a mixture of POPC and LPS (ratio 4:1) was used to mimic the Gram-negative bacterial OM (E. coli). The liposome, polypeptide, and PNG were separately dispersed into a 10 mM 2-(Nmorpholino)ethanesulfonic acid buffer (at pH 6.5) and subjected to titration. For all experiments, the pristine polypeptide and PNG were separately taken in the cell with a constant volume (250 μ L). The liposomes were taken in a syringe and titrated against PNG and polypeptide, separately. For each experiment, each time 2 μ L of liposome was injected into the cell at a time interval of 180 s, while maintaining a constant stirring speed of 300 rpm at 37 °C. The thermodynamic parameters of each experiment were evaluated by the Gibbs free-energy equation, $\Delta G = \Delta H - T\Delta S = -RT \ln K_a$. Here, ΔG , ΔH , and ΔS represent the change of Gibbs free energy, change of enthalpy, and change of entropy, respectively. The parameters T, R, and K_a represent the temperature, gas constant, and binding constant, respectively. The ITC experiment of PNG with bacterial cells has been done in an identical way as with the liposome model. Here, we have used a freshly prepared bacterial suspension at 1×10^3 CFU/ mL. The ITC cell and syringe were meticulously sterilized with ethanol just after the use of bacteria.

ASSOCIATED CONTENT

S Supporting Information

The Supporting Information is available free of charge on the ACS Publications website at DOI: 10.1021/acsami.9b10153.

Detailed synthetic protocol, material information, and characterization techniques; synthesis of monomers and polymers; and NMR, GPC, UV-vis, MIC, MTT, livedead assay, PI assay, and ITC results of the associated samples (PDF)

AUTHOR INFORMATION

Corresponding Authors

*E-mail: sudiptapanjachem@gmail.com, Sudipta_p@utexas. edu (S.P.).

*E-mail: Santanuchat71@yahoo.com, santanu@rtc.iitkgp. ernet.in (S.C.).

ORCID

Sudipta Panja: 0000-0001-5692-450X

Santanu Chattopadhyay: 0000-0002-1227-0732

Note:

The authors declare no competing financial interest.

ACKNOWLEDGMENTS

S.P. acknowledges that the use of Zn²⁺ and arginine group to reduce toxicity was proven first in Chan-Park's (NTU) lab. This research was partially supported by the National Science Foundation through the Center for Dynamics and Control of Materials: an NSF MRSEC under Cooperative agreement no. DMR-1720595. N.A.L. acknowledges support through the Welch Foundation (F-1904).

■ REFERENCES

- (1) Lam, S. J.; O'Brien-Simpson, N. M.; Pantarat, N.; Sulistio, A.; Wong, E. H. H.; Chen, Y.-Y.; Lenzo, J. C.; Holden, J. A.; Blencowe, A.; Reynolds, E. C.; Qiao, G. G. Combating Multidrug-resistant Gram-negative Bacteria with Structurally Nanoengineered Antimicrobial Peptide Polymers. *Nat. Microbiol.* **2016**, *1*, 16162.
- (2) Bresee, J.; Bond, C. M.; Worthington, R. J.; Smith, C. A.; Gifford, J. C.; Simpson, C. A.; Carter, C. J.; Wang, G.; Hartman, J.; Osbaugh, N. A.; Shoemaker, R. K.; Melander, C.; Feldheim, D. L. Nanoscale Structure-Activity Relationships, Mode of Action, and Biocompatibility of Gold Nanoparticle Antibiotics. *J. Am. Chem. Soc.* **2014**, *136*, 5295–5300.
- (3) Infectious Diseases Society of America. The 10 x 20 Initiative: Pursuing a Global Commitment to Develop 10 New Antibacterial Drugs by 2020. *Clin. Infect. Dis.* **2010**, *50*, 1081–1083.
- (4) Chen, H.; Li, M.; Liu, Z.; Hu, R.; Li, S.; Guo, Y.; Lv, F.; Liu, L.; Wang, Y.; Yi, Y.; Wang, S. Design of Antibacterial Peptide-like Conjugated Molecule with Broad Spectrum Antimicrobial Ability. *Sci. China: Chem.* **2017**, *61*, 113–117.
- (5) Pranantyo, D.; Liu, P.; Zhong, W.; Kang, E.-T.; Chan-Park, M. B. Antimicrobial Peptide-Reduced Gold Nanoclusters with Charge-Reversal Moieties for Bacterial Targeting and Imaging. *Biomacromolecules* **2019**, *20*, 2922–2933.
- (6) Wilcock, C. J.; Stafford, G. P.; Miller, C. A.; Ryabenkova, Y.; Fatima, M.; Gentile, P.; Möbus, G.; Hatton, P. V. Preparation and Antibacterial Properties of Silver-Doped Nanoscale Hydroxyapatite Pastes for Bone Repair and Augmentation. *J. Biomed. Nanotechnol.* **2017**, *13*, 1168–1176.
- (7) Hegerova, D.; Vesely, R.; Cihalova, K.; Kopel, P.; Milosavljevic, V.; Heger, Z.; Hynek, D.; Guran, R.; Vaculovicova, M.; Sedlacek, P.; Adam, V. Antimicrobial Agent Based on Selenium Nanoparticles and Carboxymethyl Cellulose for the Treatment of Bacterial Infections. *J. Biomed. Nanotechnol.* **2017**, *13*, 767–777.

- (8) Zhang, X.; Liu, L.; Liu, R.; Wang, J.; Hu, X.; Yuan, Q.; Guo, J.; Xing, G.; Zhao, Y.; Gao, X. Specific Detection and Effective Inhibition of a Single Bacterial Species in situ Using Peptide Mineralized Au Cluster Probes. Sci. China: Chem. 2018, 61, 627-634.
- (9) Li, X.; Robinson, S. M.; Gupta, A.; Saha, K.; Jiang, Z.; Moyano, D. F.; Sahar, A.; Riley, M. A.; Rotello, V. M. Functional Gold Nanoparticles as Potent Antimicrobial Agents Against Multi-Drug-Resistant Bacteria. ACS Nano 2014, 8, 10682-10686.
- (10) Bai, H.; Yuan, H.; Nie, C.; Wang, B.; Lv, F.; Liu, L.; Wang, S. A Supramolecular Antibiotic Switch for Antibacterial Regulation. Angew. Chem., Int. Ed. Engl. 2015, 54, 13208-13213.
- (11) Wu, Z.-M.; Liu, S.-Z.; Cheng, X.-Z.; Zhao, X.-R.; Hong, H.-F. High Yield Synthesis of Cyclic Analogues of Antibacterial Peptides P-113 by Sortase A-mediated Ligation and their Conformation Studies. Chin. Chem. Lett. 2017, 28, 553-557.
- (12) Zhang, T.-Y.; Li, C.; Tian, Y.-S.; Li, J.-J.; Sun, L.-P.; Zheng, C.-J.; Piao, H.-R. Synthesis and Biological Evaluation of Dihydrotriazine Derivatives as Potential Antibacterial Agents. Chin. Chem. Lett. 2017, 28, 1737-1742.
- (13) Lienkamp, K.; Madkour, A. E.; Musante, A.; Nelson, C. F.; Nüsslein, K.; Tew, G. N. Antimicrobial Polymers Prepared by ROMP with Unprecedented Selectivity: A Molecular Construction Kit Approach. J. Am. Chem. Soc. 2008, 130, 9836-9843.
- (14) Wang, C. K.; King, G. J.; Conibear, A. C.; Ramos, M. C.; Chaousis, S.; Henriques, S. T.; Craik, D. J. Mirror Images of Antimicrobial Peptides Provide Reflections on Their Functions and Amyloidogenic Properties. J. Am. Chem. Soc. 2016, 138, 5706-5713.
- (15) Zasloff, M. Antimicrobial peptides of multicellular organisms. Nature 2002, 415, 389-395.
- (16) Ilker, M. F.; Nüsslein, K.; Tew, G. N.; Coughlin, E. B. Tuning the Hemolytic and Antibacterial Activities of Amphiphilic Polynorbornene Derivatives. J. Am. Chem. Soc. 2004, 126, 15870-15875.
- (17) Exley, S. E.; Paslay, L. C.; Sahukhal, G. S.; Abel, B. A.; Brown, T. D.; McCormick, C. L.; Heinhorst, S.; Koul, V.; Choudhary, V.; Elasri, M. O.; Morgan, S. E. Antimicrobial Peptide Mimicking Primary Amine and Guanidine Containing Methacrylamide Copolymers Prepared by Raft Polymerization. Biomacromolecules 2015, 16,
- (18) Li, J.; Zhang, K.; Ruan, L.; Chin, S. F.; Wickramasinghe, N.; Liu, H.; Ravikumar, V.; Ren, J.; Duan, H.; Yang, L.; Chan-Park, M. B. Block Copolymer Nanoparticles Remove Biofilms of Drug-Resistant Gram-Positive Bacteria by Nanoscale Bacterial Debridement. Nano Lett. 2018, 18, 4180-4187.
- (19) Harvey, A. C.; Madsen, J.; Douglas, C. W. I.; MacNeil, S.; Armes, S. P. Antimicrobial Graft Copolymer Gels. Biomacromolecules **2016**. 17. 2710-2718.
- (20) Locock, K. E. S.; Michl, T. D.; Valentin, J. D. P.; Vasilev, K.; Hayball, J. D.; Qu, Y.; Traven, A.; Griesser, H. J.; Meagher, L.; Haeussler, M. Guanylated Polymethacrylates: a Class of Potent Antimicrobial Polymers with Low Hemolytic Activity. Biomacromolecules 2013, 14, 4021-4031.
- (21) Beyth, N.; Houri-Haddad, Y.; Baraness-Hadar, L.; Yudovin-Farber, I.; Domb, A. J.; Weiss, E. I. Surface Antimicrobial Activity and Biocompatibility of Incorporated Polyethylenimine Nanoparticles. Biomaterials 2008, 29, 4157-4163.
- (22) Li, Y.; Liu, G.; Wang, X.; Hu, J.; Liu, S. Enzyme-Responsive Polymeric Vesicles for Bacterial-Strain-Selective Delivery of Antimicrobial Agents. Angew. Chem., Int. Ed. Engl. 2016, 55, 1760-1764.
- (23) Liu, L.; Xu, K.; Wang, H.; Tan, P. K. J.; Fan, W.; Venkatraman, S. S.; Li, L.; Yang, Y.-Y. Self-assembled Cationic Peptide Nanoparticles as an Efficient Antimicrobial Agent. Nat. Nanotechnol. 2009, 4, 457-463.
- (24) Rahman, M. A.; Bam, M.; Luat, E.; Jui, M. S.; Ganewatta, M. S.; Shokfai, T.; Nagarkatti, M.; Decho, A. W.; Tang, C. Macromolecularclustered Facial Amphiphilic Antimicrobials. Nat. Commun. 2018, 9, 5231.
- (25) Muñoz-Bonilla, A.; Fernández-García, M. Polymeric Materials with Antimicrobial Activity. Prog. Polym. Sci. 2012, 37, 281-339.

- (26) Tew, G. N.; Scott, R. W.; Klein, M. L.; Degrado, W. F. De Novo Design of Antimicrobial Polymers, Foldamers, and Small Molecules: From Discovery to Practical Applications. Acc. Chem. Res. 2009, 43, 30-39.
- (27) Zhang, J.; Chen, Y. P.; Miller, K. P.; Ganewatta, M. S.; Bam, M.; Yan, Y.; Nagarkatti, M.; Decho, A. W.; Tang, C. Antimicrobial Metallopolymers and their Bioconjugates with Conventional Antibiotics Against Multidrug-resistant Bacteria. J. Am. Chem. Soc. 2014, 136, 4873-4876.
- (28) Chin, W.; Zhong, G.; Pu, Q.; Yang, C.; Lou, W.; De Sessions, P. F.; Periaswamy, B.; Lee, A.; Liang, Z. C.; Ding, X.; Gao, S.; Chu, C. W..; Bianco, S.; Bao, C.; Tong, Y. W.; Fan, W.; Wu, M.; Hedrick, J. L.; Yang, Y. Y. A Macromolecular Approach to Eradicate Multidrug Resistant Bacterial Infections while Mitigating Drug Resistance onset. Nat. Commun. 2018, 9, 917.
- (29) Qi, G.-B.; Zhang, D.; Liu, F.-H.; Qiao, Z.-Y.; Wang, H. An "On-Site Transformation" Strategy for Treatment of Bacterial Infection. Adv. Mater. 2017, 29, 1703461.
- (30) Zeng, L.; Wu, Y.; Xu, J.-F.; Wang, S.; Zhang, X. Supramolecular Switching Surface for Antifouling and Bactericidal Activities. ACS Appl. Bio Mater. 2019, 2, 638-643.
- (31) Li, X.; Bai, H.; Yang, Y.; Yoon, J.; Wang, S.; Zhang, X. Supramolecular Antibacterial Materials for Combatting Antibiotic Resistance. Adv. Mater. 2019, 31, 1805092.
- (32) Zheng, K.; Setyawati, M. I.; Lim, T.-P.; Leong, D. T.; Xie, J. Antimicrobial Cluster Bombs: Silver Nanoclusters Packed with Daptomycin. ACS Nano 2016, 10, 7934-7942.
- (33) Peng, B.; Zhang, X.; Aarts, D. G. A. L.; Dullens, R. P. A. Superparamagnetic Nickel Colloidal Nanocrystal Clusters with Antibacterial Activity and Bacteria Binding Ability. Nat. Nanotechnol. 2018, 13, 478-482.
- (34) Pasquet, J.; Chevalier, Y.; Pelletier, J.; Couval, E.; Bouvier, D.; Bolzinger, M.-A. The Contribution of Zinc Ions to the Antimicrobial Activity of Zinc Oxide. Colloids Surf., A 2014, 457, 263-274.
- (35) Liu, S. Q.; Yang, C.; Huang, Y.; Ding, X.; Li, Y.; Fan, W. M.; Hedrick, J. L.; Yang, Y.-Y. Antimicrobial and Antifouling Hydrogels Formed in Situ from Polycarbonate and Poly(ethylene glycol) via Michael Addition. Adv. Mater. 2012, 24, 6484-6489.
- (36) Xu, Q.; Zheng, Z.; Wang, B.; Mao, H.; Yan, F. Zinc Ion Coordinated Poly(Ionic Liquid) Antimicrobial Membranes for Wound Healing. ACS Appl. Mater. Interfaces 2017, 9, 14656-14664.
- (37) Epand, R. M.; Rotem, S.; Mor, A.; Berno, B.; Epand, R. F. Bacterial Membranes as Predictors of Antimicrobial Potency. J. Am. Chem. Soc. 2008, 130, 14346-14352.
- (38) Panja, S.; Dey, G.; Bharti, R.; Kumari, K.; Maiti, T. K.; Mandal, M.; Chattopadhyay, S. Tailor-Made Temperature-Sensitive Micelle for Targeted and On-Demand Release of Anticancer Drugs. ACS Appl. Mater. Interfaces 2016, 8, 12063-12074.
- (39) Panja, S.; Maji, S.; Maiti, T. K.; Chattopadhyay, S. A Smart Magnetically Active Nanovehicle for on-Demand Targeted Drug Delivery: Where van der Waals Force Balances the Magnetic Interaction. ACS Appl. Mater. Interfaces 2015, 7, 24229-24241.
- (40) Panja, S.; Maji, S.; Maiti, T. K.; Chattopadhyay, S. A Branched Polymer as a pH Responsive Nanocarrier: Synthesis, Characterization and Targeted Delivery. Polymer 2015, 61, 75-86.
- (41) Zasloff, M. Antimicrobial Peptides of Multicellular Organism. Nature 2002, 415, 389-395.
- (42) Schmidt, N. W.; Mishra, A.; Lai, G. H.; Davis, M.; Sanders, L. K.; Tran, D.; Garcia, A.; Tai, K. P.; McCray, P. B.; Ouellette, A. J.; Selsted, M. E.; Wong, G. C. L. Criterion for Amino Acid Composition of Defensins and Antimicrobial Peptides Based on Geometry of Membrane Destabilization. J. Am. Chem. Soc. 2011, 133, 6720-6727.
- (43) Panja, S.; Dey, G.; Bharti, R.; Mandal, P.; Mandal, M.; Chattopadhyay, S. Metal Ion Ornamented Ultrafast Light-Sensitive Nanogel for Potential in Vivo Cancer Therapy. Chem. Mater. 2016, 28, 8598-8610.
- (44) Hou, Z.; Shankar, Y. V.; Liu, Y.; Ding, F.; Subramanion, J. L.; Ravikumar, V.; Zamudio-Vázquez, R.; Keogh, D.; Lim, H.; Tay, M. Y. F.; Bhattacharjya, S.; Rice, S. A.; Shi, J.; Duan, H.; Liu, X.-W.; Mu, Y.;

- Tan, N. S.; Tam, K. C.; Pethe, K.; Chan-Park, M. B. Nanoparticles of Short Cationic Peptidopolysaccharide Self-Assembled by Hydrogen Bonding with Antibacterial Effect Against Multidrug-Resistant Bacteria. ACS Appl. Mater. Interfaces 2017, 9, 38288–38303.
- (45) Bharti, R.; Dey, G.; Ojha, P. K.; Rajput, S.; Jaganathan, S. K.; Sen, R.; Mandal, M. Diacerein-mediated Inhibition of IL-6/IL-6R Signaling Induces Apoptotic Effects on Breast Cancer. *Oncogene* **2016**, 35, 3965–3975.
- (46) Morrow, B. J.; Abbanat, D.; Baum, E. Z.; Crespo-Carbone, S. M.; Davies, T. A.; He, W.; Shang, W.; Queenan, A. M.; Lynch, A. S. Antistaphylococcal Activities of the New Fluoroquinolone JNJ-Q2. *Antimicrob. Agents Chemother.* **2011**, *55*, 5512–5521.
- (47) Pucci, M. J.; Cheng, J.; Podos, S. D.; Thoma, C. L.; Thanassi, J. A.; Buechter, D. D.; Mushtaq, G.; Vigliotti, G. A., Jr.; Bradbury, B. J.; Deshpande, M. In vitro and In vivo Antibacterial Activities of Heteroaryl Isothiazolones Against Resistant Gram-positive Pathogens. *Antimicrob. Agents Chemother.* **2007**, *51*, 1259–1267.
- (48) Bharti, R.; Dey, G.; Ojha, P. K.; Rajput, S.; Jaganathan, S. K.; Sen, R.; Mandal, M. Diacerein-mediated Inhibition of IL-6/IL-6R Signaling Induces Apoptotic Effects on Breast Cancer. *Oncogene* **2016**, 35, 3965–3975.
- (49) Fukushima, K.; Tan, J. P. K.; Korevaar, P. A.; Yang, Y. Y.; Pitera, J.; Nelson, A.; Maune, H.; Coady, D. J.; Frommer, J. E.; Engler, A. C.; Huang, Y.; Xu, K.; Ji, Z.; Qiao, Y.; Fan, W.; Li, L.; Wiradharma, N.; Meijer, E. W.; Hedrick, J. L. Broad-Spectrum Antimicrobial Supramolecular Assemblies with Distinctive Size and Shape. ACS Nano 2012, 6, 9191–9199.
- (50) Chen, Y.-Y.; Peng, B.; Yang, Q.; Glew, M. D.; Veith, P. D.; Cross, K. J.; Goldie, K. N.; Chen, D.; O'Brien-Simpson, N.; Dashper, S. G.; Reynolds, E. C. The Outer Membrane Protein LptO is Essential for the O-Deacylation of LPS and the Co-ordinated Secretion and Attachment of A-LPS and CTD Proteins in Porphyromonas Gingivalis. *Mol. Microbiol.* **2011**, *79*, 1380–1401.